Microstructures and Mechanical Properties of Resistance Spot-Welded Steel/Aluminum Alloy Joints with Process Tapes

Yingying Che, Lei Wang, Daqian Sun, Hongmei Li, and Wenhua Geng

The microstructure and mechanical property of resistance spot-welded joints of steel and aluminum were studied by using process tapes. The steel/aluminum joint consists mainly of aluminum nugget and interface zone. The liquid nugget solidification has an epitaxial growth characteristic, and the interface zone displays a double-layer structure, Fe_2Al_5 layer at steel side and Fe_4Al_{13} layer at aluminum nugget side. Compared with joints without process tape, the joint nugget diameter and tensile shear load increased by 35.45 and 10.98%, respectively, and its indentation ratio decreased by 56.25% due to the process tapes increasing heat input, producing larger nugget diameter and continuous interface layer, and protecting against deep indentation. The joining area of intermetallic layer and aluminum nugget is weak link in the joint. It is favorable to use the process tapes for improving welding quality, raising joint strength, and energy saving.

1. Introduction

With the vigorous development of the global economy, reducing fuel consumption and gas emission has become a serious challenge for the automotive industry (Ref 1). Automotive lightweight is recognized as the most direct and effective way for that above, which has been a hot innovation topic of automobile manufacturers (Ref 2). Under the premise of ensuring the body safety, replacing steel with aluminum alloy to form a hybrid structure in the non-bearing parts of the automobile is a compromise between performance and cost (Ref 3). Consequently, the joining of dissimilar metals of steel and aluminum alloy has become the urgent problem to be solved due to their significant differences in physical and thermal properties and forming brittle Fe-Al intermetallics (IMC) at the steel/aluminum interface, which seriously deteriorates the mechanical properties of welded joints (Ref 4, 5). There are some research activities on the joining of steel and aluminum in recent years. The current methods are generally solid-state welding processes, such as the diffusion welding (Ref 6, 7), friction stir welding (Ref 8), ultrasonic welding (Ref 9, 10) and magnetic pulse welding (Ref 11, 12). However, their application is limited by the geometry and size of workpieces. Fusion welding techniques were also used for joining aluminum to steel. In 2012, Dong et al. (Ref 13) joined the aluminum alloy sheet to galvanized steel sheet using gas tungsten arc welding (GTAW). Results showed that with the increase in weld Si content the joint strength increased, but the effect of interfacial IMC layer thickness on it was opposite. According to reference (Ref 14, 15), the IMC layer thickness in the joint produced with metal inert-gas arc welding (MIG) had effect on the joint strength and it decreased obviously when the IMC layer thickness was more than 10 μm. Kouadri-David (Ref 16) focused on the metallurgic and mechanical properties of laser-welded heterogeneous joints between DP600 galvanized steel and 6082 aluminum. The joint properties could be improved by controlling the inter-sheet gap and using the keyhole mode. Experimental results of cold metal transfer welding (CMT) (Ref 17, 18) and hybrid laser welding (Ref 19-21) indicated that excessive intermetallic compounds in the interface deteriorated the steel/aluminum joint properties.

Resistance spot welding was widely used in automobile industry. Sun et al. (Ref 22) joined SAE1008 mild steel and 5182-O aluminum alloy sheets using the resistance spot welding, and introduced a cold-rolled strip material as the transition material to decrease the interfacial IMC layer thickness to below 8.5 μm. Satonaka (Ref 23) and Qiu et al. (Ref 24) studied the resistance spot welding of steel and aluminum alloy with cover plate. Based on the finite element analysis, the temperature of weld produced with cover plate was 200-300 °C higher than that without cover plate. In addition, it is also favorable to use the cover plate for energy saving. Kim et al. (Ref 25) welded DP590 and Al5052 by using Delta-spot welding process. As results, the delta-spot welding process adopting process tapes was beneficial for the improvement of the joint strength. The authors studied effects of the electrode morphology and welding parameter on resistance spot-welded joints of high strength steel and aluminum alloy (Ref 26, 27). The results showed that optimizing the electrode morphology and welding parameter are effective ways

Yingying Che, Daqian Sun, Hongmei Li, and **Wenhua Geng**, Key Laboratory of Automobile Materials, Ministry of Education, School of Materials Science and Engineering, Jilin University, No. 5988 Renmin Street, Changchun 130025, People's Republic of China; **Lei Wang**, Key Laboratory of Automobile Materials, Ministry of Education, School of Materials Science and Engineering, Jilin University, No. 5988 Renmin Street, Changchun 130025, People's Republic of China; and Changchun Automobile Industry Institute, Changchun 130011, People's Republic of China. Contact e-mails: cheyingying123@126.com, 36531698@163.com, sundq@jlu.edu.cn, lihongmei0511@126.com, and 18635017879@163.com.

for improving microstructures and mechanical properties of steel/aluminum joints. The present work investigates the resistance spot welding of DP980 high strength steel and 5083 aluminum alloy using process tapes. Its purpose is to better understand the weldability of dissimilar metals of steel and aluminum and to provide some foundation for improving the welding quality and joint properties.

2. Materials and Methods

The base metals used in this investigation were DP980 high strength steel and 5083 aluminum alloy sheets, the sheet thickness being 1.0 and 1.5 mm, respectively. Their chemical compositions and mechanical properties are presented in Tables 1 and 2, respectively. Figure 1 shows the shape and size of high strength steel and aluminum alloy specimens used for resistance spot welding (RSW) experiment. Prior to welding, both steel and aluminum specimens were polished with sandpapers and then washed with acetone in order to remove oxides and dirt on the specimen surfaces.

It is well known that the heat input of RSW mainly comes from the resistance heat generated by electric current flowing through workpieces. Because the aluminum has larger electrical conductivity (62%I.A.C.S.) and thermal conductivity (222 W/m K) than steel, the more heat input is required for RSW of steel and aluminum. Figure 2 shows the schematic diagrams of resistance spot welding without process tape and with process tapes. The RSW with process tape can generate more resistance heat than traditional RSW without process tape due to adding the body resistance of process tape and the contact resistance

between process tape and workpieces. In this experiment, the austenitic stainless steel and carbon steel process tapes with thickness of 0.3 mm (Fig. 2b, c, and d), the OI delta-spot median frequency direct current welding system (Fig. 3) and the flat copper alloy electrodes with tip diameter of 16 mm were used for welding of steel and aluminum. The welding parameters were the welding current of 11-16 kA, welding time of 100-300 ms, electrode force of 5 kN, pre-squeezed force of 3 kN and pre-squeezed time of 50 ms, respectively. The microstructural characteristics of steel/aluminum joints with process tapes and effects of welding conditions on the joints were studied by changing the process tape and welding parameter. The steel/aluminum joints without process tape were also prepared in order to evaluate their advantages and disadvantages for welding of steel and aluminum.

After welding, the metallographic samples of joints were cut into the size of 15 mm × 10 mm through the weld center. Then, they were ground, polished, and finally etched with Keller reagent to reveal the joint macrostructure and microstructure. The microstructures, and chemical and phase compositions of the joints were examined by using scanning electron microscope (SEM, EVO18) equipped with an energy-dispersive x-ray spectroscopy (EDS, Link-ISIS), microregion x-ray diffraction (M-XRD, X'Pert3 Powder) and transmission electron microscope (TEM, JEM-2100F). The joint nugget diameter, IMC layer thickness and indentation depth were measured under optical microscope (Zeiss Scope A1) and SEM. The indentation ratio was calculated by following equation:

$$\delta = d_1 + d_2/t_1 + t_2 \tag{Eq 1}$$

where δ is indentation ratio, t_1 and d_1 are thickness and indentation depth of steel sheet, respectively, and t_2 and d_2

Table 1 Chemical compositions of base metals (wt.%)

Aluminum	Si 0.21	Fe 0.25	Cu 0.06	Mn0.75	Mg 4.35	Cr 0.11	Zn 0.12	Ti 0.05	Al Bal.
Steel	C ≤ 0.23	Mn ≤ 3.00	P ≤ 0.04	Si ≤ 0.60	S ≤ 0.015	Al ≥ 0.010	…	…	Fe Bal.

Table 2 Mechanical properties of base metals

Base metal	Yield strength, MPa	Tensile strength, MPa	Elongation, %
DP980 steel	550	980	7
5083 aluminum	120	297	17
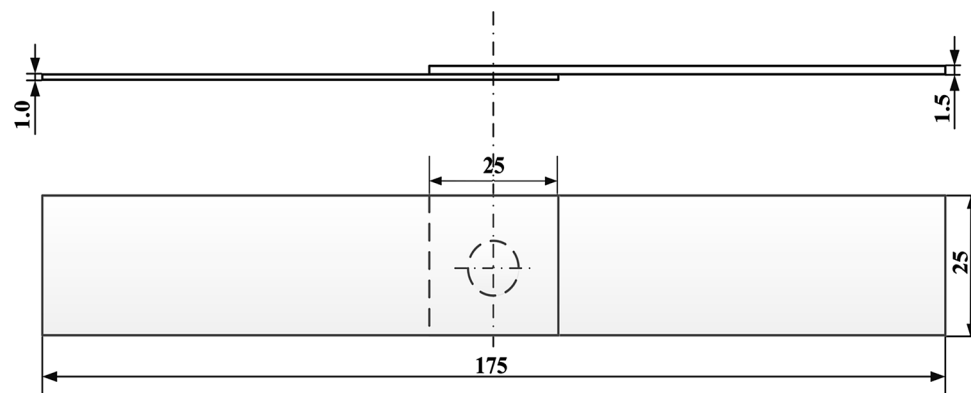
Fig. 1 The shape and size of specimens used for resistance spot welding experiment
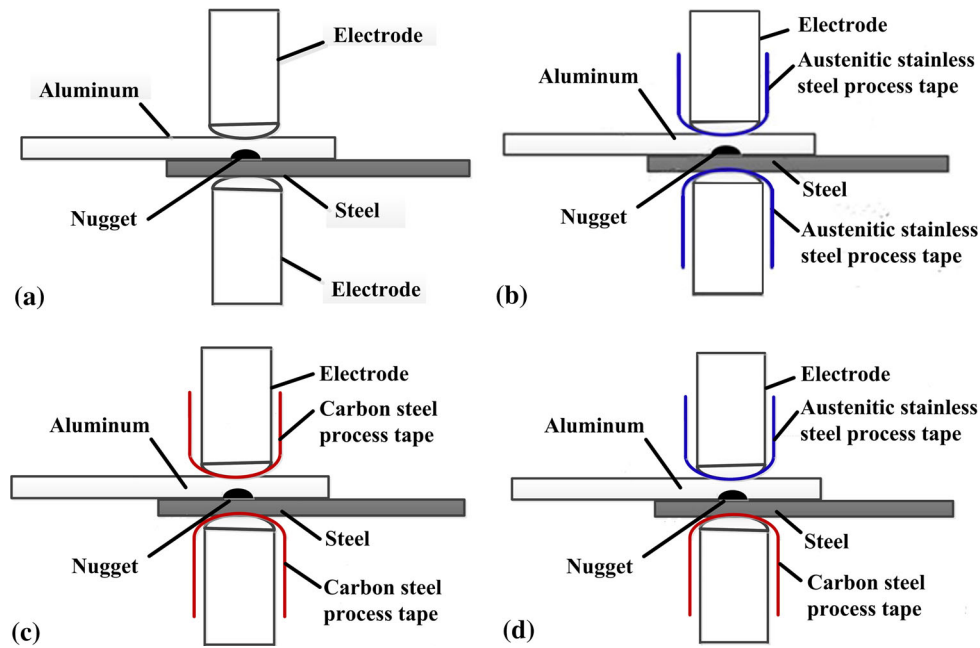
Fig. 2 Schematic diagrams of resistance spot welding. (a) Without process tape, (b) with stainless steel process tape, (c) with carbon steel process tape, (d) with stainless steel process tape on aluminum side and carbon steel process tape on steel side

**Fig. 3** The resistance spot welding machine used in the experiment

are thickness and indentation depth of aluminum sheet, respectively. The tensile shear test was carried out using a MTS 810 material testing system. The joint tensile shear load was determined based on the average value of three measurements per condition. After the tensile shear test, the joint fractured surface was examined using SEM.

3. Results and Discussion

3.1 Joint Microstructures

Figure 4 illustrates the cross-sectional macrostructure and microstructure of resistance spot-welded joint of DP980 steel and 5083 aluminum with process tapes. From Fig. 4a, it can be

seen that the joint consists mainly of aluminum alloy nugget and steel/aluminum interface zone. Owing to great differences of melting temperatures between steel and aluminum, during welding the aluminum alloy was melted locally to form liquid state nugget while the steel remained solid state. The aluminum was joined to steel by the reactive diffusion between liquid aluminum and solid steel. Therefore, the steel/aluminum joint has welding-brazing characteristics. Figure 4(b) and (c) shows microstructures of aluminum nugget, corresponding to regions A and B in Fig. 4(a), respectively. The liquid aluminum nugget solidified epitaxially from aluminum base metal grains and α-Al cellular crystals tended to grow in the direction perpendicular to the fusion line (Fig. 4b), because it is the direction of the maximum temperature gradient and hence maximum heat extraction. With further advance of solid/liquid interface toward
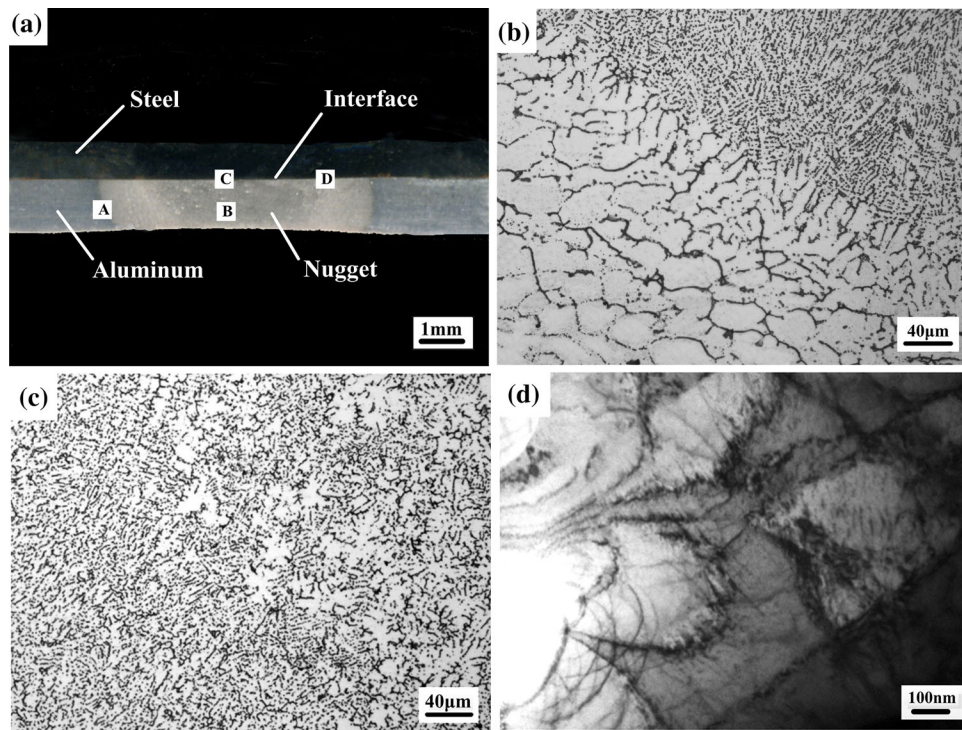
Fig. 4 The macrostructure and microstructure of joint. (a) Joint macrostructure, (b) microstructure of region A, (c) microstructure of region B, (d) TEM image of dislocations

to the pool center, the solidification mode changed from cellular crystal to cellular dendrite, and finally to equiaxed dendrite, as shown in Fig. 4(c). It can be explained by the degree of constitutional supercooling continuing to increase. Figure 4(d) presents TEM bright field image of aluminum nugget. Tangled dislocations were observed, which is related to the formed tensile stress in the nugget during welding.

Figure 5 shows microstructures, EDS line-scan and XRD results of steel/aluminum interface zone. Figure 5(a) and (b) corresponds to microstructures of regions C and D in Fig. 5(a), respectively. There exists an interface layer between steel base metal and aluminum nugget. It displays a tongue-like structure close to the steel base metal and a fine needle-like structure close to the aluminum nugget. From interfacial center to its edge, the interface layer thickness has a decreased tendency, as shown in Fig. 5(a) and (b). The welding heat input has an evident effect on the interface layer. At low heat input, the interface layer was discontinuous and there existed interface defects (Fig. 5c). Increasing the heat input tended to decrease the interface defect and finally form the continuous interface layer (Fig. 5d). EDS line-scan results showed that the inter-diffusion of Fe and Al across steel/aluminum interface occurred during welding, resulting in heterogeneous distribution of Fe and Al. From steel side to aluminum side, the Fe concentration reduced while the Al concentration enhanced in the interface layer (Fig. 5a). According to micro-XRD results shown in Fig. 5(e), the diffraction peaks of Fe_2Al_5 are obvious, but because the Fe_4Al_{13} is much less than the Fe_2Al_5 in the interface layer and the minimum selected area of micro-XRD is much larger than the interface layer thickness, the diffraction peaks of Fe_4Al_{13} are very weak. TEM was used to reveal more detailed microstructural characteristics of the interface layer. Figure 6 shows TEM bright field image and selected area diffraction patterns of the interface layer.

From Fig. 6(a), it can be seen that the interface zone has a double-layer structure: the tongue-like Fe_2Al_5 layer at steel base metal side (Fig. 6b) and needle-like Fe_4Al_{13} layer at aluminum nugget side (Fig. 6c). The formation of Fe_4Al_{13} phase was confirmed by the TEM results. The reaction between Fe and Al atoms can generate Fe_3Al, FeAl, $FeAl_2$, Fe_2Al_5 and Fe_4Al_{13} intermetallic compounds. According to the thermodynamic data (Ref 28), the relationship of standard Gibbs's free energy (ΔG^θ) of their formation is $\Delta G^\theta(Fe_3Al) > \Delta G^\theta(FeAl) > \Delta G^\theta(FeAl_2) > \Delta G^\theta(Fe_2Al_5) > \Delta G^\theta(Fe_4Al_{13})$. Therefore, it is easier to form Fe_2Al_5 and Fe_4Al_{13} due to their formation requiring less energy. In addition, the growth of the intermetallic compounds also depends on the formation kinetics. Fe_2Al_5 phase has faster growth rate compared with Fe_4Al_{13} phase, because its growth kinetics coefficient (e.g., 2.30×10^{-6} m s^{-2}, 800 °C) is larger than Fe_4Al_{13} (e.g., 0.12×10^{-6} m s^{-2}, 800 °C) (Ref 29, 30).

Based on characteristics of the joint microstructure, the reactive diffusion of liquid aluminum alloy and solid steel is necessary for joining aluminum to steel. At low heat input, forming discontinuous IMC layer is mainly attributed to insufficient reactive diffusion. It is harmful to mechanical properties of steel/aluminum joint because the interface defect not only decreases the joint effective cross section but also accelerates the nucleation and propagation of cracks under tensile shear load. Therefore, forming continuous interface layer should favor the improvement of joint properties.

3.2 Effects of Welding Conditions

The welding conditions are important factors affecting the welding quality and joint properties. Therefore, effects of process tapes and welding parameters on the steel/aluminum joints were studied in this experiment.
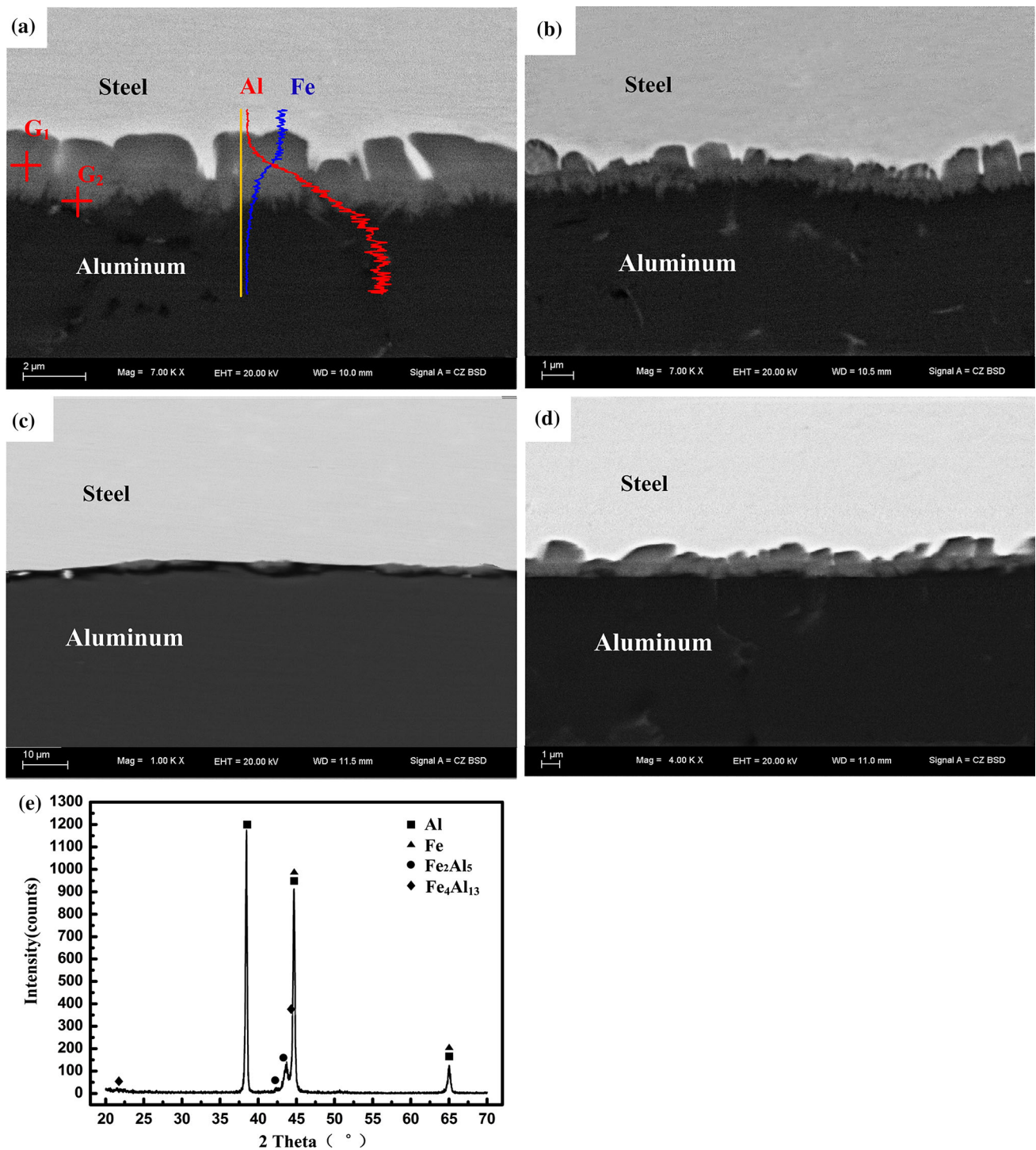
Fig. 5 Microstructures, EDS and XRD results of interface zone. (a) Microstructure and EDS result of region C, (b) microstructure of region D, (c) interface defect, (d) continuous interface layer, (e) XRD result

3.2.1 Effects of Process Tapes. When traditional resistance spot welding (RSW) without process tape was used (Fig. 2a), some problems were encountered in dissimilar joining of steel and aluminum. Firstly, due to the metallurgical reaction between copper electrode and aluminum alloy sheet during welding, the electrode tip was polluted by adherent copper-aluminum alloy, as shown in Fig. 7(a) and (b), which leads to decreasing the electrode service life and RSW

production efficiency. Secondly, during welding the severe expulsion and deep indentation occurred on the aluminum side (Fig. 7c), affecting not only welding process stability but also joint surface quality. Finally, the more welding heat input (or larger welding machine capacity) was required because of the aluminum having large electrical conductivity and thermal conductivity. In this investigation, it was found that RSW of steel and aluminum using process tapes is helpful for solving
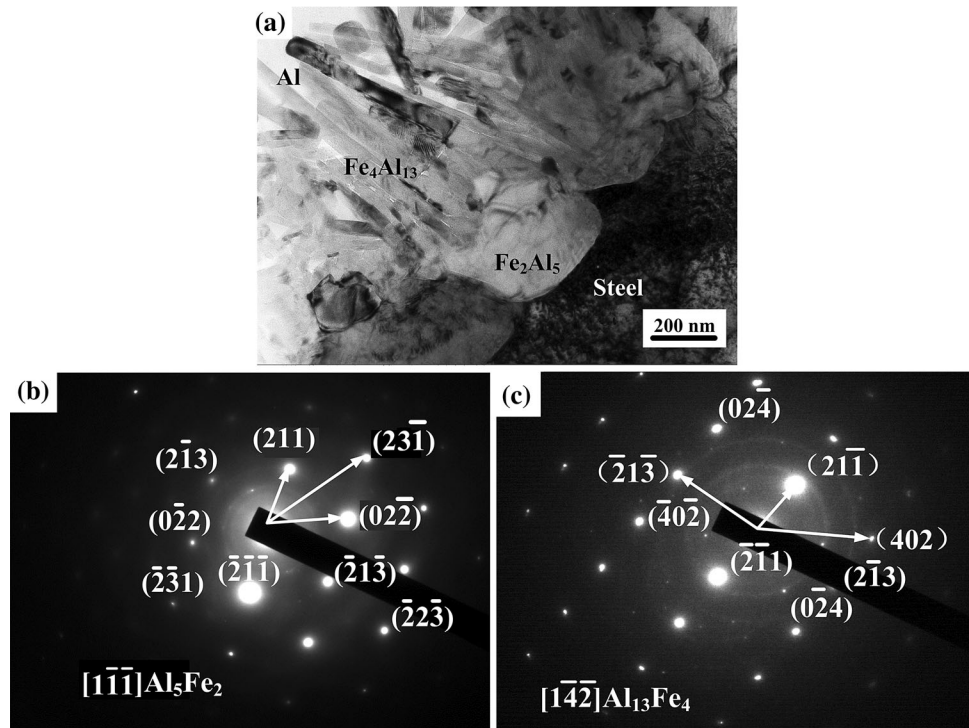
Fig. 6 TEM bright field image and selected area diffraction patterns of interface zone. (a) TEM image, (b) Fe₂Al₅ diffraction pattern, (c) Fe₄Al₁₃ diffraction pattern

the problems mentioned above. It can avoid the metallurgical reaction of the copper and aluminum, and reduce obviously the electrode adhesion, welding expulsion and indentation depth (Fig. 7d), which favors improving the electrode service life and welding quality. The reduced welding expulsion is related to avoiding the reaction of copper and aluminum. In addition, it is also favorable to use the process tape for increasing welding heat input because of adding the body resistance of process tape and the contact resistance between process tape and workpieces.

The experimental results indicated that the chemical composition and position placed of process tapes had great influence on welding quality. When the austenitic stainless steel process tape was used (Fig. 2b), the reaction of the copper and aluminum was avoided, but the process tape between the copper electrode and steel sheet easily adhered to the steel surface, as shown in Fig. 8(a). It is mainly associated with the austenitic stainless steel having small electrical conductivity and thermal conductivity, hence generating excessive resistance heat. When the carbon steel process tape was used (Fig. 2c), Owing to it having larger electrical conductivity than the stainless steel, the process tape adhesion was avoided (Fig. 8b), but the aluminum nugget had a decreased tendency compared with using stainless steel process tape, which is unfavorable for mechanical properties of the joint. Based on the experiment results, it is more favorable to place stainless steel and carbon steel process tapes in aluminum and steel sides, respectively (Fig. 2d) for improving welding quality and joint properties.

3.2.2 Effects of Welding Parameters. The welding current and welding time are important RSW parameters. Effects of welding current on the steel/aluminum joints with and without process tapes were studied under the condition of

constant welding time (300 ms) and electrode force (5 kN). The stainless steel and carbon steel process tapes were placed in aluminum and steel sides, respectively, in this experiment (Fig. 2d). Figure 9 shows cross sections of the joints at various welding currents. As can be seen, the joints produced with process tapes have bigger aluminum nugget compared with those without process tape. The process tapes increase resistance heat (heat input). The larger the heat input is, the higher the joint temperature (Ref 23), hence forming bigger aluminum nugget. When the welding current exceeded 13 kA (without process tape) and 15 kA (with process tapes), the excessive welding heat input expanded the liquid aluminum nugget rapidly, generating the welding spatter. The loss of liquid aluminum resulted in insufficient liquid metal filling the nugget and forming shrinkage porosities after the liquid nugget solidification, as shown in Fig. 9(c) and (f). The lower welding heat input in other welding current conditions made the amount of melted aluminum smaller, prevented welding spatter from occurrence during the welding under the action of the electrode force, and hence there was no shrinkage porosity in the aluminum nuggets.

Figure 10 shows effects of welding current on the nugget diameter, interface IMC layer thickness, indentation ratio and tensile shear load of steel/aluminum joints. From Fig. 10(a), (b), and (c) with the increase in welding current from 11 to 16 kA, the nugget diameter, IMC layer thickness and indentation ratio of the joints with process tapes increased from 5.31 mm, 1.12 μm and 4.08% to 10.43 mm, 2.83 μm and 7.00%, and those of joints without process tape increased from 5.30 mm, 0.80 μm and 6.70% to 7.70 mm, 1.16 μm and 16.00%, respectively. The joints with process tapes have larger nugget diameter and IMC layer thickness and smaller inden-
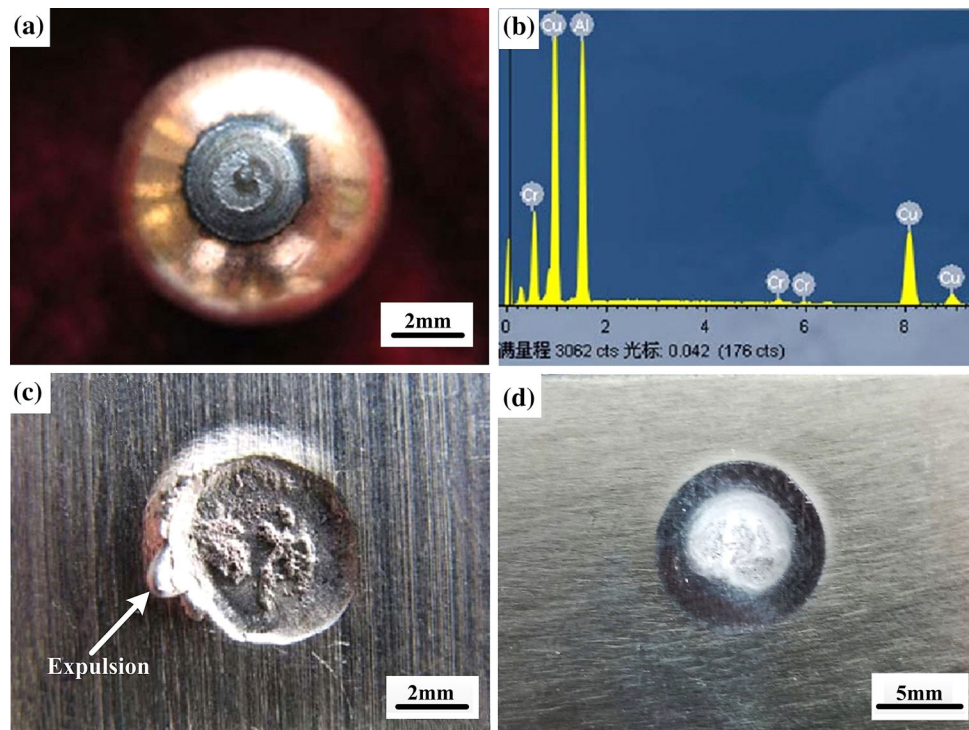
Fig. 7 The surface morphology of electrode tip and joints (a) electrode tip morphology, (b) electrode tip EDS analysis, (c) joint surface morphology without process tape and (d) joint surface morphology with austenitic stainless steel process tape on aluminum side and carbon steel process tape on steel side
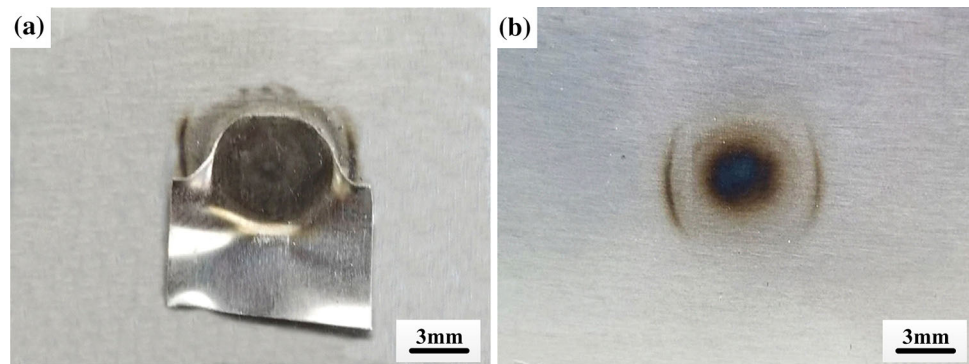

Fig. 8 The surface morphology of joints on the steel side (a) with austenitic stainless steel process tape and (b) with carbon steel process tape

tation ratio than those without process tape. Under the condition of same welding current (16 kA), the nugget diameter and IMC thickness of joint with process tapes increased by 35.45 and 143.97%, respectively, and its indentation ratio reduced by 56.25% compared with those of joints without process tape, which is related to the process tapes increasing heat input and protecting against deep indentation on steel and aluminum sheets. At the same nugget diameter of 7.50 mm, the welding current required with process tapes reduced by 25.0% compared with that without process tape. It is also related to the process tapes increasing the heat input. It should be pointed out that the process tape affects not only IMC layer thickness but also its morphology. With the process tape, the double-layer structure characteristic of IMC is more obvious and it is also favorable for forming continuous IMC layer due to increasing welding heat input.

Figure 10(d) presents the effect of welding current on tensile shear load of the joints. At relatively low welding current (11 kA) the joint gave poor tensile shear load, which is mainly attributed to the low heat input producing small nugget diameter and discontinuous IMC layer (Fig. 5c). The joint tensile shear load increased with the increase in welding current, due to increasing the nugget diameter, decreasing the interface defect and forming the continuous interface layer. The maximum tensile shear load reached 4.10 kN (without process tape) and 4.55 kN (with process tapes) at welding current of 13 and 15 kA, respectively. With further increase in welding current, the joint tensile shear load had a decreased tendency. It can be explained by increasing welding spatter and indentation depth and forming shrinkage porosities in the joints.
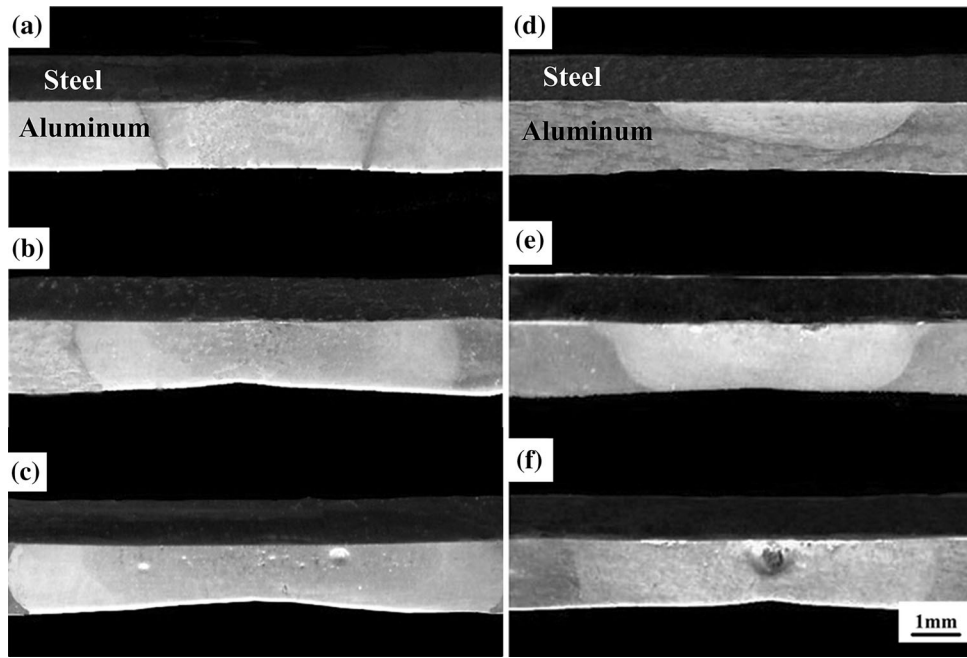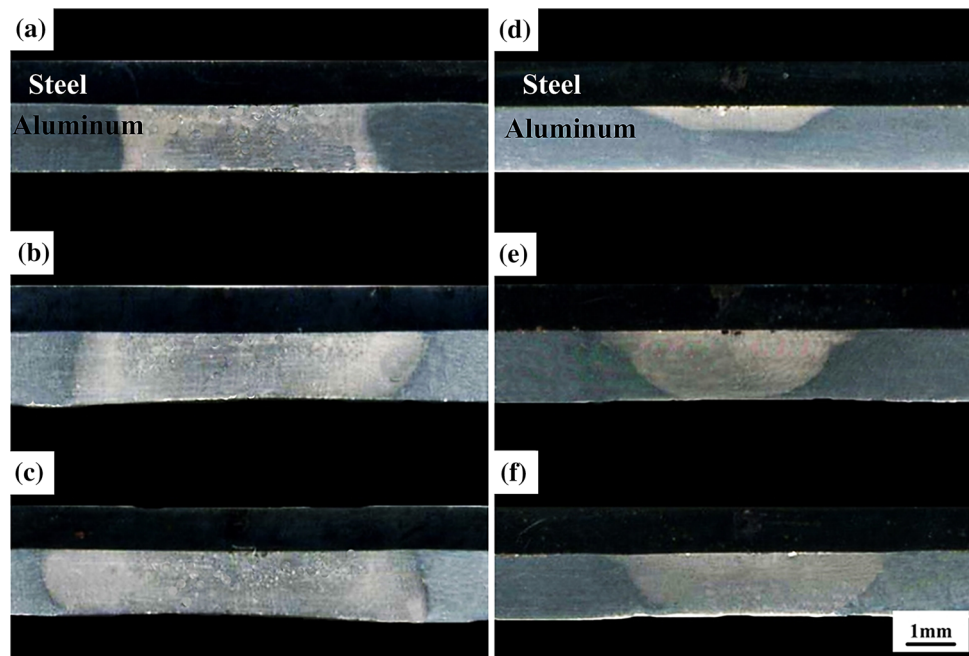
Fig. 9 Cross sections of joints at various welding currents with process tapes and without process tape (a) 11 kA, (b) 13 kA, (c) 16 kA (with austenitic stainless steel process tape on aluminum side and carbon steel process tape on steel side), and (d) 11 kA, (e) 13 kA, (f) 15 kA (without process tape)
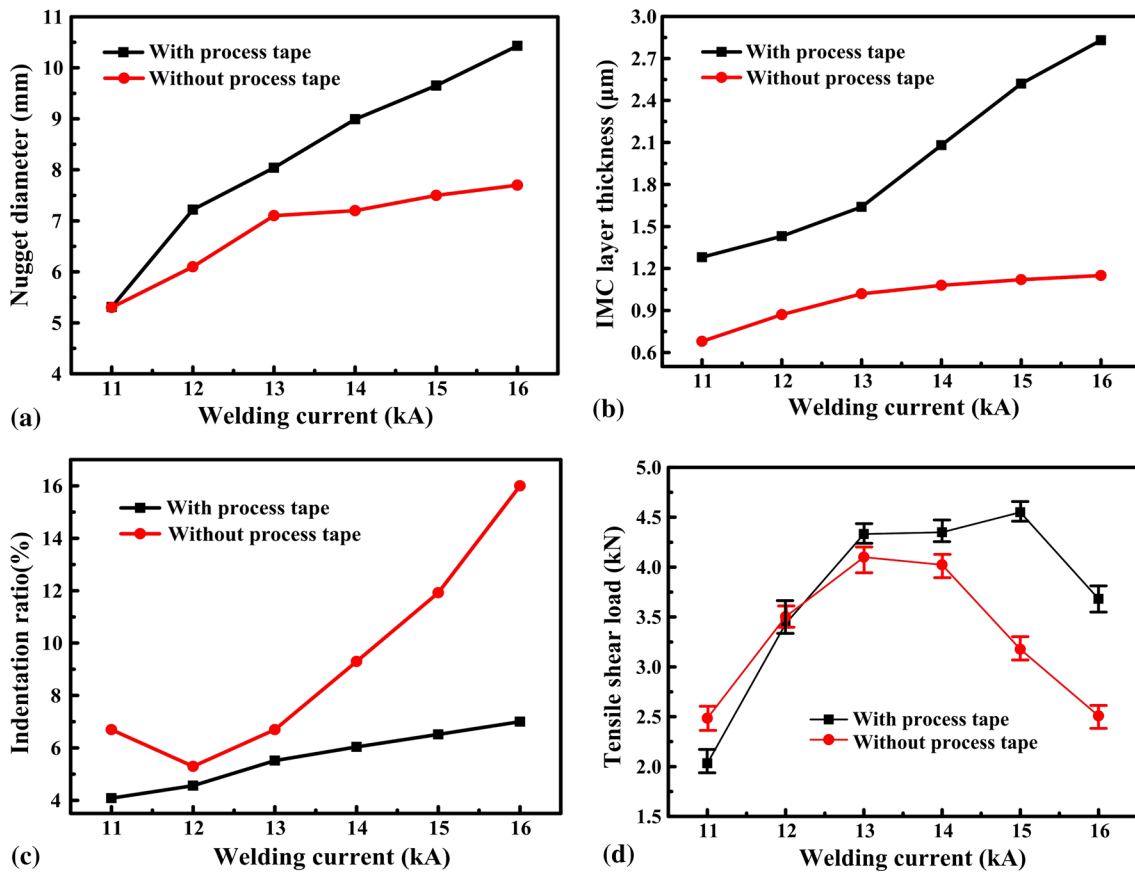
Fig. 10 Effects of welding current on (a) nugget diameter, (b) IMC layer thickness, (c) indentation ratio and (d) tensile shear load of joints with and without process tapes

Fig. 11 Cross sections of joints at various welding time with process tapes and without process tape (a) 100 ms, (b) 200 ms, (c) 300 ms (with austenitic stainless steel process tape on aluminum side and carbon steel process tape on the steel side), and (d) 100 ms, (e) 200 ms, (f) 300 ms (without process tape)

Effects of welding time on steel/aluminum joints with and without process tapes were studied under the condition of constant welding current (13 kA) and electrode force (5 kN). Figures 11 and 12 show cross sections of joints at various welding time and effects of welding time on the joints, respectively. With the increase in welding time from 100 to 300 ms, the nugget diameter, IMC thickness and tensile shear load of joints with and without process tapes increased, they reaching to 8.10 mm, 1.64 μm and 4.32 kN (with process tapes) and 7.10 mm, 1.02 μm and 4.10 kN (without process tape), respectively, at welding time of 300 ms. Under the condition of same welding time (300 ms), the nugget diameter, IMC layer thickness and tensile shear load of joint with process tapes increased by 14.08, 60.78 and 5.37%, respectively, compared with those without process tape. At the same nugget diameter of 7.00 mm, the welding time required with process tapes was shortened 33.33% compared with that without process tape.

Figure 13 shows relationships of joint tensile shear load with nugget diameter and IMC layer thickness. The experimental results indicated that the nugget diameter had great effect on the joint tensile shear load. It increased obviously with the increase in nugget diameter (Fig. 13a), demonstrating that the nugget diameter is main factor affecting the joint strength. It was well known that Fe-Al intermetallics are very brittle. Increasing IMC layer thickness means increasing the brittle intermetallics in the steel/aluminum interface, which should be disadvantageous for the joint properties. However, in this investigation it was found that the joint tensile shear load displayed an increased tendency with IMC layer thickness increasing from 0.51 to 2.83 μm, as shown in Fig. 13(b). It is related to decreasing the interface defect and forming the continuous IMC layer.

Based on results above, the welding conditions have obvious effects on the steel/aluminum joints. Under the condition of this experiment, producing larger nugget diameter and continuous interface layer by increasing heat input is an effective approach for improving the joint strength. Compared to the maximum tensile shear load (4.10 kN) of joint without process tape, that (4.55 kN) with process tapes increased by 10.98%. Compared with RSW without process tape, the RSW with process tapes is more favorable for improving the welding quality, joint properties and production efficiency, due to its advantages such as increasing the heat input, nugget diameter and joint tensile shear load, and decreasing the indentation ratio, welding current and welding time required.

3.3 Joint Fracture Mode

Figure 14 shows morphologies of cracks in the steel/aluminum joint under the action of different tensile shear loads. As shown in Fig. 14(a), the interface defect is a preferential site for crack initiation due to its tip producing stress concentration under the tensile shear load. In addition, the crack also initiated in the edge of Fe_4Al_{13} intermetallic layer just adjacent to aluminum alloy nugget, as shown in Fig. 14(b). With the increase in tensile shear load the crack propagated mainly along the edge of the IMC layer (Fig. 14c), not in its inside in spite of the IMC layer having high brittleness, and it could propagate into the aluminum nugget when the larger tensile shear load was applied, as shown in Fig. 14(d). These results suggested that the joining area of brittle IMC layer and plastic aluminum nugget is weak link in the steel/aluminum joint. It is mainly related to their great differences in chemical, physical and mechanical properties.
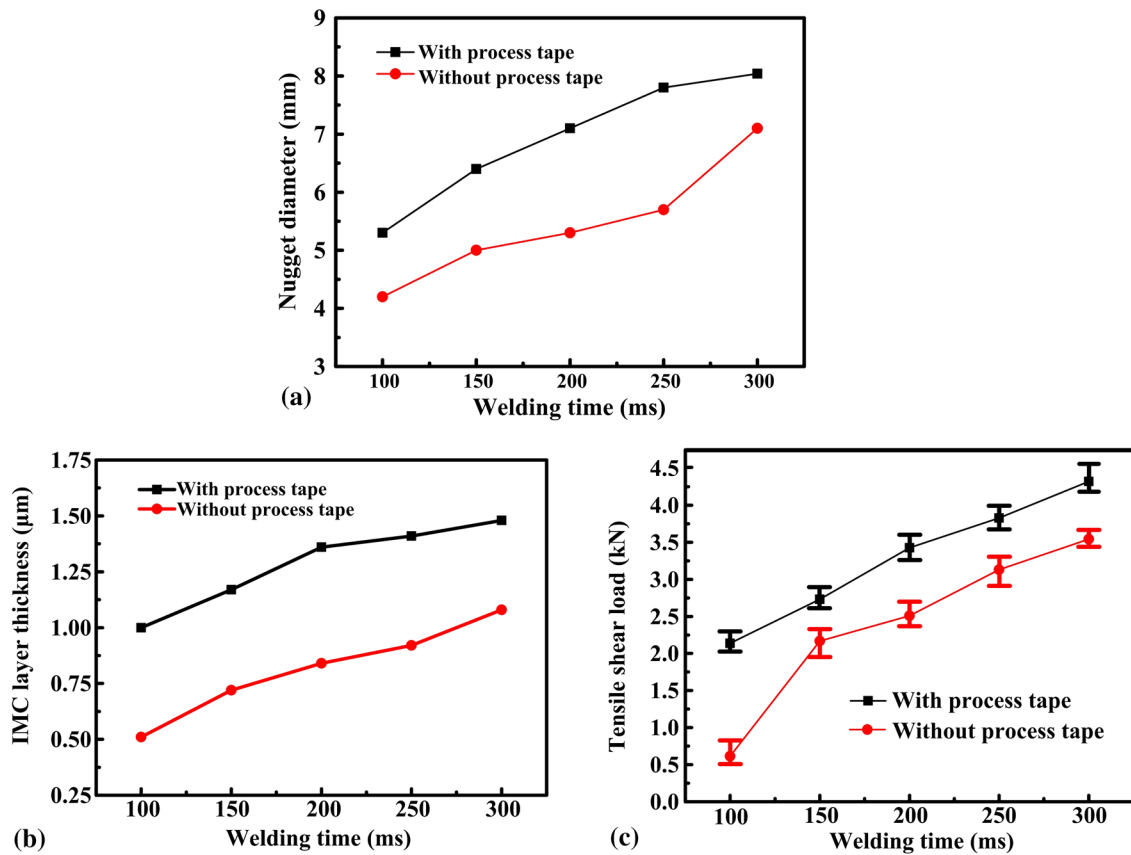
Fig. 12 Effects of welding current on (a) nugget diameter, (b) IMC layer thickness, and (c) tensile shear load of joints with and without process tapes
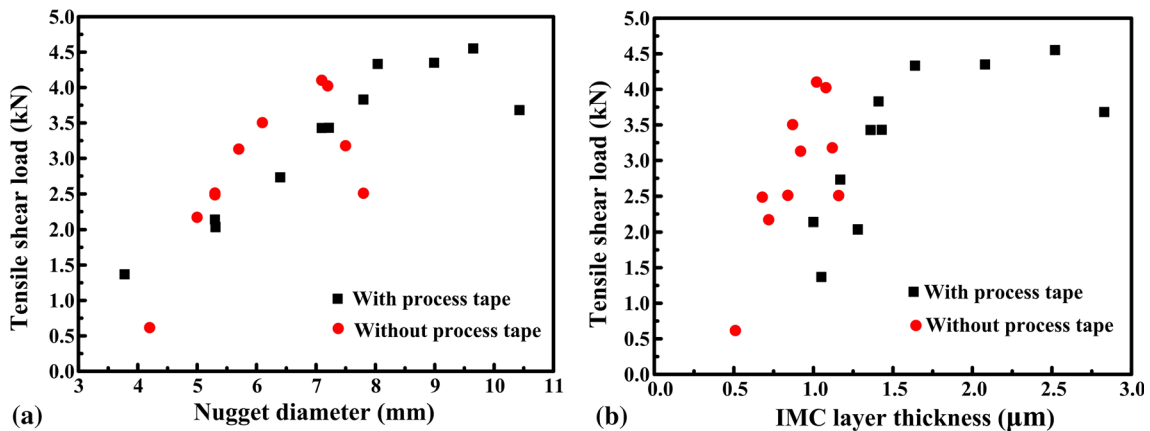

Fig. 13 Relationships of joint tensile shear load with (a) nugget diameter and (b) IMC layer thickness

Figure 15(a) illustrates typical fracture surface morphology of steel/aluminum joint on steel side. Figure 15(b) and (c) presents the enlarged images of regions A and B in Fig. 15(a), respectively. The fracture surface of region A is relatively flat and mainly contains Fe, Al and Mg elements, as shown in Fig. 15(b). EDS analysis results indicated that atom percents of the region A are 76.79 at.%Al, 22.08 at.% Fe and 1.13% Mg, which corresponds to Fe_4Al_{13} intermetallic interval in the Fe-Al binary alloy phase diagram.

Therefore, in the region A the joint fracture occurred in the joining area of IMC layer and aluminum nugget. In contrast to the region A, the region B displays different fracture surface morphology. The dimples with different sizes and tear-shaped marks along the dimple boundaries were observed, as shown in Fig. 15(c). Its Al content is more than 95 at.% based on EDS analysis results, indicating that in the region B the joint fracture occurred in the aluminum nugget. From the enlarged image shown in Fig. 15(d), it can be seen
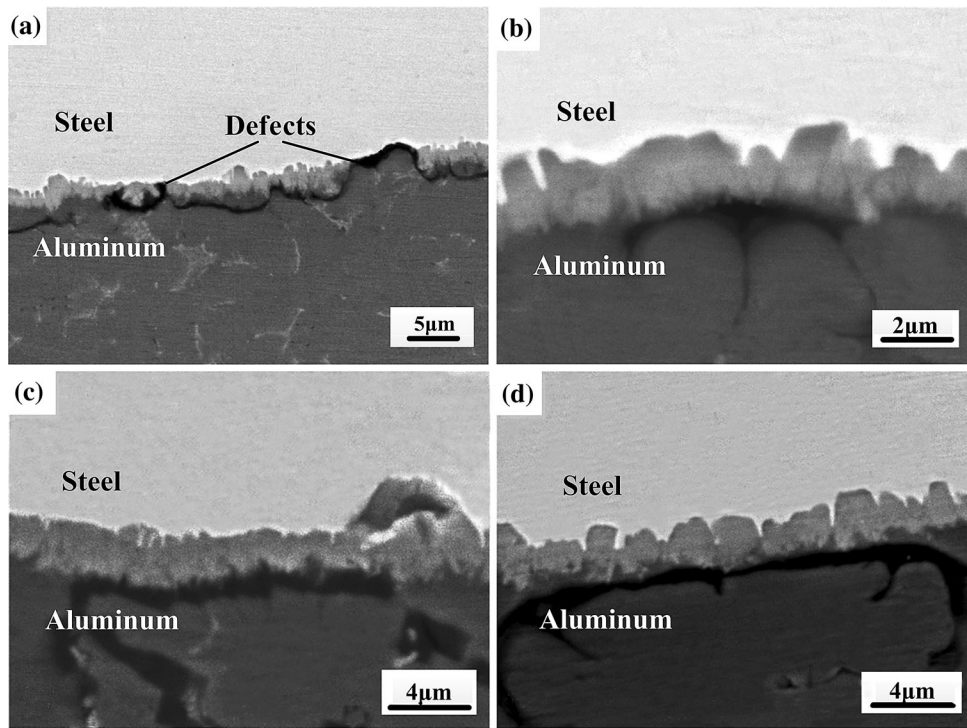
Fig. 14 Morphologies of cracks in the joints under the different tensile shear loads. (a) 1.0 kN, (b) 2.0 kN, (c) 3.0 kN and (d) 4.0 kN
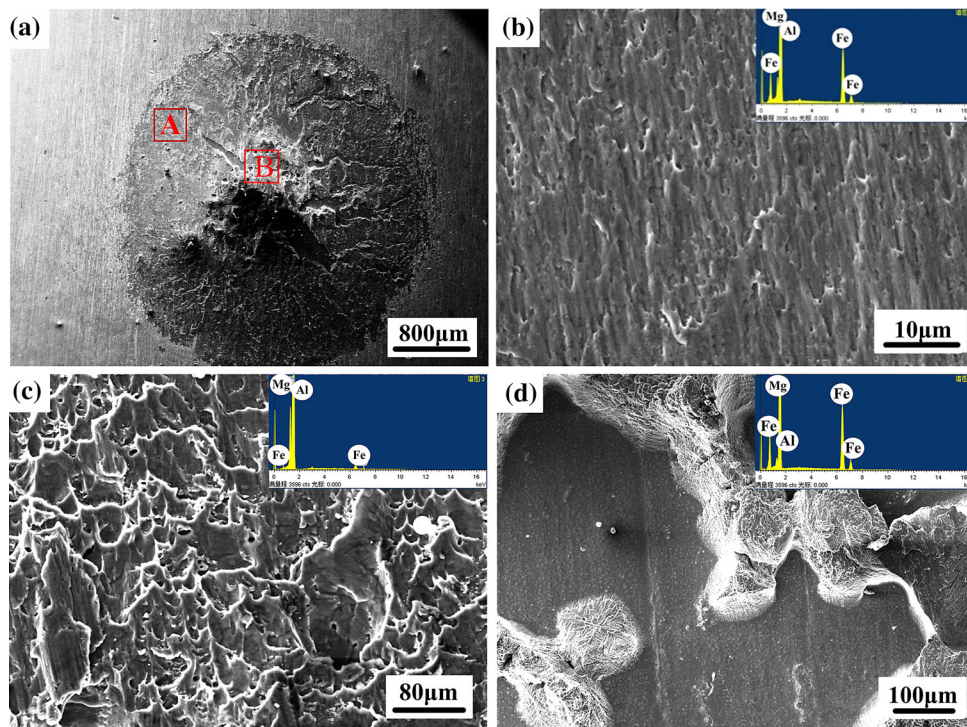
Fig. 15 Fracture surface morphologies of joint on steel side. (a) Fracture surface morphology, (b) enlarged image of region A, (c) enlarged image of region B, (d) enlarged image of interface defect

that there exists fine interface defect in the joint, meaning that wetting of liquid aluminum on steel surface and steel/aluminum interface reaction did not occur in this region. The result suggested that it is also favorable to improve the wetting ability of liquid aluminum on steel surface for increasing the joint strength.

4. Conclusions

1. Resistance spot-welded steel/aluminum joint with process tapes consists mainly of aluminum nugget and interface zone. The liquid nugget solidified epitaxially from the aluminum base metal, and its solidification mode changes from cellular crystal to cellular dendrite, and finally to equiaxed dendrite due to the constitutional supercooling degree increasing. During welding, the reactive diffusion between liquid aluminum and solid steel occurs to form Fe-Al IMC layers, the Fe_2Al_5 layer at steel side and Fe_4Al_{13} layer at aluminum nugget side. The low heat input produces discontinuous IMC layer because of insufficient reactive diffusion, which is harmful to the joint properties.

2. The process tape has great influence on the resistance spot welding of steel and aluminum. It can effectively avoid the metallurgical reaction between copper electrode and aluminum sheet, protect against the electrode adhesion, severe expulsion and deep indentation, and can also decrease the welding current and welding time required at same nugget diameters due to increasing welding heat input. It is more favorable to place austenitic stainless steel and carbon steel process tapes in aluminum and steel sides, respectively, for improving welding quality, saving energy and raising efficiency.

3. The process tape has an obvious influence on the steel/aluminum joint. Compared with joints without process tape, the nugget diameter and tensile shear load of joints with process tapes increased by 35.45 and 10.98%, respectively, and its indentation ratio decreased by 56.25%, which is related to the process tape increasing heat input and protecting against deep indentation. The process tape increasing joint strength is mainly associated with increasing nugget diameter and forming continuous interface layer. The joining area of IMC layer and aluminum nugget is weak link in the steel/aluminum joint. It is also favorable to use the process tape for improving the mechanical properties of the steel/aluminum joint.

References

1. J. Sun, Q. Yan, W. Gao, and J. Huang, Investigation of Laser Welding on Butt Joints of Al/Steel Dissimilar Materials, *Mater. Des.*, 2015, **83**, p 120-128

2. R. Hörhold, M. Müller, M. Merklein, and G. Meschut, Mechanical Properties of an Innovative Shear-Clinching Technology for Ultra-High-Strength Steel and Aluminium in Lightweight Car Body Structures, *Weld. World*, 2016, **60**, p 1-8

3. A. Bouayad, Ch Gerometta, A. Belkebir, and A. Ambair, Kinetic Interactions Between Solid Iron and Molten Aluminum, *Mater. Sci. Eng. A*, 2003, **363**, p 53-61

4. G. Sierra, P. Peyre, F.D. Beaume, D. Stuart, and G. Fras, Galvanised Steel to Aluminium Joining by Laser and GTAW Processes, *Mater. Charact.*, 2008, **59**(12), p 1705-1715

5. S.W. Mei, M. Gao, J. Yan, C. Zhang, G. Li, and X.Y. Zeng, Interface Properties and Thermodynamic Analysis of Laser-Arc Hybrid Welded Al/Steel Joint, *Sci. Technol. Weld. Join.*, 2013, **18**, p 293-300

6. M.K. Karfoul, G.J. Tatlock, and R.T. Murray, The Behaviour of Iron and Aluminium During the Diffusion Welding of Carbon Steel to Aluminium, *J. Mater. Sci.*, 2007, **42**(14), p 5692-5699

7. H. Shi, S. Qiao, R. Qiu, and X.Z.H. Yu, Effect of Welding Time on the Joining Phenomena of Diffusion Welded Joint Between Aluminum Alloy and Stainless Steel, *Mater. Manuf. Process.*, 2012, **27**(12), p 1366-1369

8. S. Kundu, D. Roy, R. Bhola, D. Bhattacharjee, and B. Mishra, Microstructure and Tensile Strength of Friction Stir Welded Joints Between Interstitial Free Steel and Commercially Pure Aluminium, *Mater. Des.*, 2013, **50**, p 370-375

9. M. Shakil, N.H. Tariq, M. Ahmad, M.A. Choudhary, J.I. Akhter, and S.S. Babue, Effect of Ultrasonic Welding Parameters on Microstructure and Mechanical Properties of Dissimilar Joints, *Mater. Des.*, 2014, **55**(6), p 263-273

10. T. Watanabe, H. Sakuyama, and A. Yanagisawa, Ultrasonic Welding Between Mild Steel Sheet and Al-Mg Alloy Sheet, *J. Mater. Process. Technol.*, 2009, **209**(15-16), p 5475-5480

11. H. Yu, Z. Xu, Z. Fan, Z. Zhao, and C. Li, Mechanical Property and Microstructure of Aluminum Alloy-Steel Tubes Joint by Magnetic Pulse Welding, *Mater. Sci. Eng. A Struct.*, 2013, **561**(3), p 259-265

12. J.Y. Shim, I.S. Kim, K.J. Lee, and B.Y. Kang, Experimental and Numerical Analysis on Aluminum/Steel Pipe Using Magnetic Pulse Welding, *Met. Mater. Int.*, 2011, **17**(6), p 957-961

13. H. Dong, W. Hu, Y. Duan, X. Wang, and C. Dong, Dissimilar Metal Joining of Aluminum Alloy to Galvanized Steel with Al-Si, Al-Cu, Al-Si-Cu and Zn-Al Filler Wires, *J. Mater. Process. Technol.*, 2012, **212**, p 458-464

14. H. Zhang and J. Liu, Microstructure Characteristics and Mechanical Property of Aluminum Alloy/Stainless Steel Lap Joints Fabricated by MIG Welding-Brazing Process, *Mater. Sci. Eng. A*, 2011, **528**, p 6179-6185

15. Q. Chang, D. Sun, X. Gu, and H. Li, Microstructures and Mechanical Properties of Metal Inert-Gas Arc Welded Joints of Aluminum Alloy and Ultrahigh Strength Steel Using Al-Mg and Al-Cu Fillers, *J. Mater. Res.*, 2017, **32**(3), p 666-676

16. A. Kouadri-David, Study of Metallurgic and Mechanical Properties of Laser Welded Heterogeneous Joints Between DP600 Galvanised Steel and Aluminium 6082, *Mater. Des.*, 2014, **54**(54), p 184-195

17. R. Cao, J.H. Sun, J.H. Chen, and P.C. Wang, Cold Metal Transfer Joining of Aluminum AA6061-T6-to-Galvanized Boron Steel, *J. Manuf. Sci. E*, 2014, **136**(5), p 351-373

18. Y.B. Liu, Q.J. Sun, J.P. Liu, S.J. Wang, and J.C. Feng, Effect of Axial External Magnetic Field on Cold Metal Transfer Welds of Aluminum Alloy and Stainless Steel, *Mater. Lett.*, 2015, **152**, p 29-31

19. Z. Lei, X. Wang, A. You, G. Qin, W. Wang, and S.Y. Lin, Research on Fusion-Brazing Joining Between Aluminum and Steel by Laser-MIG Hybrid Welding, *Rare Met. Mater. Eng.*, 2009, **38**(12), p 229-233

20. C. Thomy and F. Vollertsen, Laser-Mig Hybrid Welding of Aluminium to Steel—Effect of Process Parameters on Joint Properties, *Weld. World*, 2012, **56**(5-6), p 124-132

21. J. Yan, M. Gao, and X.Y. Zeng, Study on Microstructure and Mechanical Properties of 304 Stainless Steel Joints by TIG, Laser and Laser-TIG Hybrid Welding, *Opt. Lasers Eng.*, 2010, **48**(4), p 512-517

22. X. Sun, E.V. Stephens, M.A. Khaleel, H. Shao, and M. Kimchi, Resistance Spot Welding of Aluminum Alloy to Steel with Transition Material-From Process to Performance, *Weld. J.*, 2004, **83**, p 188s-195s

23. S. Satonaka, C. Iwamoto, R. Qui, and T. Fujioka, Trends and New Applications of Spot Welding for Aluminium Alloy Sheets, *Weld. Int.*, 2006, **20**(11), p 858-864

24. R. Qiu, C. Iwamoto, and S. Satonaka, Interfacial Microstructure and Strength of Steel/Al Alloy Joints Welded by RSW with Cover Plate, *J. Mater. Process. Technol.*, 2009, **209**(8), p 4186-4193

25. J.S. Kim, I.J. Kim, and Y.G. Kim, Optimization of Welding Current Waveform for Dissimilar Material with DP590 and Al5052 by Delta-Spot Welding Process, *J. Mech. Sci. Technol.*, 2016, **30**(6), p 2713-2721

26. W. Zhang, D. Sun, L. Hana, and Y. Li, Optimised Design of Electrode Morphology for Novel Dissimilar Resistance Spot Welding of

Aluminium Alloy and Galvanised High Strength Steel, *Mater. Des.*, 2015, **85**, p 461-470

27. D. Sun, Y. Zhang, Y. Liu, G. Xiaoyan, and H. Li, Microstructures and Mechanical Properties of Resistance Spot Welded Joints of 16 Mn Steel and 6063-T6 Aluminum Alloy with Different Electrodes, *Mater. Des.*, 2016, **109**, p 596-608

28. L.Z. Cheng and Y.H. Zhang, *Physical Chemistry*, Shanghai Science & Technology Press, Shanghai, 2007, p 3

29. K. Bouché, F. Barbier, and A. Coulet, Intermetallic Compound Layer Growth Between Solid Iron and Molten Aluminium, *Mater. Sci. Eng. A*, 1998, **249**(1-2), p 167-175

30. W. Zhang, D. Sun, L. Han et al., Characterization of Intermetallic Compounds in Dissimilar Material Resistance Spot Welded Joint of High Strength Steel and Aluminum Alloy, *Trans. Iron Steel Inst. Jpn.*, 2011, **51**(11), p 1870-1877